

A large-scale traveling ionospheric disturbance during the magnetic storm of 15 September 1999

K. Shiokawa,¹ Y. Otsuka,¹ T. Ogawa,¹ N. Balan,² K. Igarashi,³ A. J. Ridley,⁴
D. J. Knipp,⁵ A. Saito,⁶ and K. Yumoto⁷

Received 31 July 2001; revised 16 October 2001; accepted 16 October 2001; published 29 June 2002.

[1] Using a comprehensive data set and model calculations, we have investigated a prominent large-scale traveling ionospheric disturbance (LSTID) observed in Japan ($\sim 37^\circ$ – 16° MLAT) on 15 September 1999, during a recovery phase of sequential storms. The LSTID was detected at 2300–2400 LT (1400–1500 UT) as an enhancement of the 630-nm airglow intensity (50→350 R), a decrease in the F layer virtual height (at 2 MHz, 360→200 km), an enhancement of f_oF_2 (6→8 MHz), and an enhancement of GPS total electron content ($\sim 1.0 \times 10^{16} \text{ m}^{-2}$). Multipoint and imaging observations of these parameters show that the LSTID moved equatorward over Japan with a velocity of ~ 400 – 450 m/s. From a comparison with the Sheffield University Plasmasphere-Ionosphere Model (SUPIM) we conclude that an enhancement (250–300 m/s) of poleward neutral wind (that is propagating equatorward) caused these observational features of the LSTID at midlatitudes. To investigate generation of the LSTID by auroral energy input, we have used auroral images obtained by the Polar UVI instrument, magnetic field variations obtained at multipoint ground stations, and the empirical Joule heating rate calculated by the assimilative mapping of ionospheric electrodynamics (AMIE) technique. Intense auroral energy input was observed at 0800–1100 UT (4–6 hours before the LSTID), probably causing equatorward neutral wind at lower latitudes. It is likely that the poleward wind pulse that caused the observed LSTID was generated associated with the cessation of this equatorward wind. The effect of Lorentz force is also discussed.

INDEX TERMS: 0310 Atmospheric Composition and Structure: Airglow and aurora; 2427 Ionosphere: Ionosphere/atmosphere interactions (0335); 2435 Ionosphere: Ionospheric disturbances; 2437 Ionosphere: Ionospheric dynamics; 2788 Magnetospheric Physics: Storms and substorms; **KEYWORDS:** large-scale traveling ionospheric disturbance, thermosphere–ionosphere coupling, magnetic storm, airglow imaging, GPS network, ionosonde

1. Introduction

[2] Large-scale traveling ionospheric disturbances (LSTIDs) observed during magnetic storms were investigated throughout the second half of the last century. They have a horizontal size of more than 1000 km and propagate equatorward with a velocity of 400–1000 m/s [Hunsucker, 1982]. These disturbances are probably caused by atmospheric gravity waves generated by the auroral-zone energy input [Hooke, 1968; Francis, 1975]. Observations of LSTIDs up to 1995 have been reviewed by Hunsucker

[1982] and Hocke and Schlegel [1996]. Pi et al. [2000] have reported comprehensive radar and optical measurements of the storm time ionosphere, and they observed large-scale equatorward moving gravity waves induced by auroral heating. Afraimovich et al. [2000] determined LSTID parameters using GPS arrays. However, few observations of LSTID have been made using recently developed imaging techniques, such as O I (630 nm) airglow images [e.g., Mendillo et al., 1997] and the multipoint GPS network [e.g., Saito et al., 1998]. Ho et al. [1996, 1998] obtained a two-dimensional image of the LSTIDs as global total electron content (TEC) maps using the multipoint GPS network.

[3] Several simulations have shown the equatorward propagation of gravity waves from the auroral-zone energy input [e.g., Richmond, 1978; Millward et al., 1993; Fuller-Rowell et al., 1994; Fujiwara et al., 1996; Balthazor and Moffett, 1999]. Most of the simulations show dominant enhancement of equatorward wind and associated upward motion of the ionosphere in the midlatitudes during the LSTID passage. The rise of the F layer has been confirmed by observations [e.g., Tanaka, 1987; Hajkowicz and Hun-

¹Solar-Terrestrial Environment Laboratory, Nagoya University, Toyokawa, Japan.

²Department of Physics, University of Wales, Aberystwyth, U.K.

³Communications Research Laboratory, Koganei, Tokyo, Japan.

⁴University of Michigan, Ann Arbor, Michigan, USA.

⁵Department of Physics, U.S. Air Force Academy, Colorado, USA.

⁶Graduate School of Science, Kyoto University, Kyoto, Japan.

⁷Faculty of Science, Kyushu University, Fukuoka, Japan.

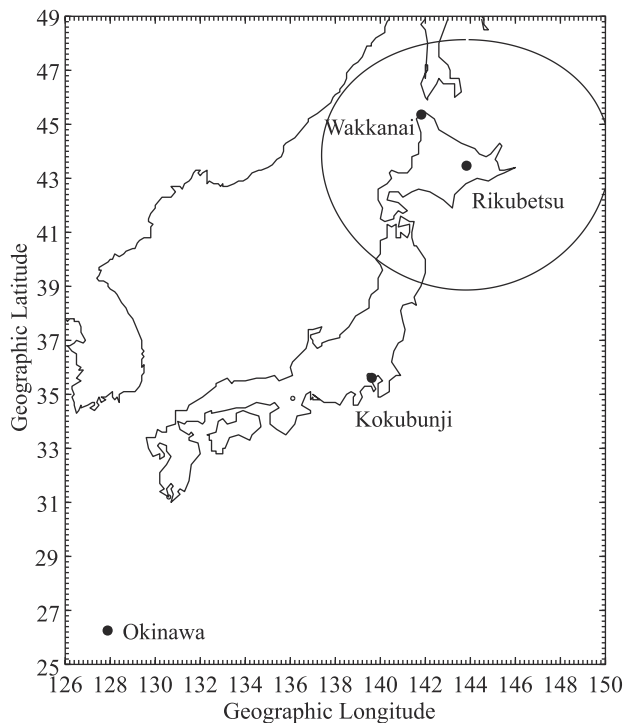


Figure 1. Map showing the locations of stations. The airglow data shown in Figures 3 and 4 were obtained at Rikubetsu (magnetic latitude (MLAT) = 34.7°), where the field of view of the airglow imaging (radius of 500 km) is also shown. The ionogram data shown in Figure 5 were obtained at Wakkanai (36.5° MLAT), Kokubunji (26.5° MLAT), and Okinawa (16.3° MLAT).

sucker, 1987; Hajkowicz, 1990]. The event shown in this paper, however, is characterized by a drastic F layer descent and an associated airglow enhancement.

[4] As reviewed by Hunsucker [1982], two possible causes of LSTIDs, i.e., the Lorentz force and the Joule heating, can be considered in the auroral zone. The recent development of an inversion technique from ground magnetometer data to the ionospheric current makes it possible to calculate a global map of auroral current and the associated Joule heating rate [Kamide *et al.*, 1981; Richmond and Kamide, 1988]. Emery *et al.* [1996, 1999], Buonsanto *et al.* [1997], and Lu *et al.* [2001] combined these empirical models of auroral energy input with the thermosphere-ionosphere electrodynamics general circulation model (TIEGCM) to describe storm time thermospheric disturbances and LSTID generations.

[5] In this paper, we report a prominent LSTID event observed in Japan during the magnetic storm of 15 September 1999. We use two-dimensional airglow images, ionograms obtained at three Japanese stations, and two-dimensional TEC maps obtained by more than 1000 GPS receivers over Japan. The observed ionospheric parameters are compared with results obtained from an ionospheric model with poleward wind enhancement. The source of the LSTID in the auroral zone is investigated using auroral images obtained by the Polar UVI instrument, multipoint ground-based magnetograms, and auroral energy input

estimated by the assimilative mapping of ionospheric electrodynamics (AMIE) technique.

2. Observations

[6] Figure 1 shows the locations of the ground-based stations where the LSTID was observed. The airglow enhancement was observed at Rikubetsu (43.5°N , 143.8°E , geomagnetic latitude (MLAT) = 34.7°). Ionosonde measurements were made at Wakkanai (45.4°N , 141.7°E ; 36.5° MLAT), Kokubunji (35.7°N , 139.5°E ; 26.5° MLAT), and Okinawa (26.3°N , 127.8°E ; 16.3° MLAT). The latitudinally extended chain stations enable us to observe north-south motion of the LSTID.

[7] Figure 2 shows Dst indices during the magnetic storm of 12–15 September 1999. Three sequential storms occurred in this interval, i.e., from 0900 UT on 12 September from 2000 UT on 13 September and from 2200 UT on 14 September to 2200 UT on 15 September. The LSTID event reported here was observed during the last storm activity on 15 September, as shown by the vertical dashed line.

2.1. Midlatitude Airglow

[8] The all-sky imager and the meridian-scanning photometer used in the present study were developed in the Solar-Terrestrial Environment Laboratory, Nagoya University, as part of the Optical Mesosphere Thermosphere Imagers (OMTI) [Shiokawa *et al.*, 1999, 2000]. Figure 3 shows variations in airglow intensity at the O I 630-nm line, observed by a meridian-scanning photometer at Rikubetsu on the night of 15 September 1999. A clear enhancement of airglow intensity is seen at 1300–1500 UT (2200–2400 LT). The enhancement was first observed to the north of Rikubetsu and then moved to the south. The maximum intensity of the enhancement at zenith was ~ 350 R. It is unusual to observe such intense airglow emission at mid-latitude stations. Assuming that the altitude of the airglow emission was 250 km, we estimate the velocity of the southward motion to be ~ 450 m/s from the photometer data.

[9] Figure 4 shows all-sky images of 630-nm airglow obtained at Rikubetsu during the airglow enhancement

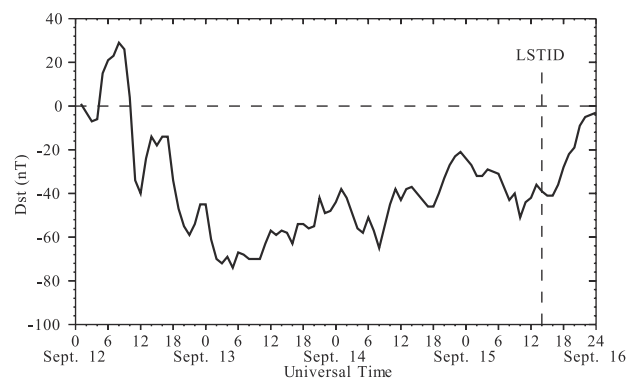


Figure 2. Four-day Dst indices during the sequential magnetic storm of 12–16 September 1999. The vertical dashed line indicates the time when the large-scale traveling ionospheric disturbance (LSTID) was observed in Japan.

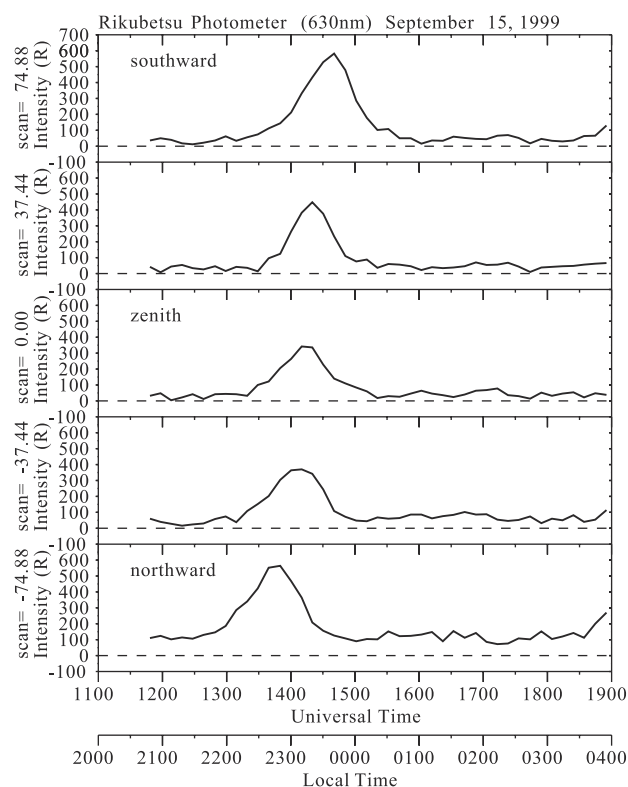


Figure 3. Variations in 630-nm airglow intensity obtained by a meridian-scanning photometer at Rikubetsu on 15 September 1999. The intensities were obtained at the five zenith angles shown at the left side of the panels. The Van Rhijn effect is not corrected in the plotted data. An airglow enhancement that reaches ~ 350 R at zenith moved from north to south at 1300–1500 UT (2200–2400 LT).

event of 15 September shown in Figure 3. Upward is to the north and left is to the east. The airglow enhancement appeared in the northern sky in the image around 1318:32 UT (2218:32 LT). It passed Rikubetsu around 1413:03 UT (2313:03 LT) to the south. It is noteworthy that the airglow enhancement was more intense in the west than in the east in the image at 1413:03 UT, indicating a longitudinal structure of the LSTID. Rough estimation gives that the airglow intensity in the west was $\sim 40\%$ larger than in the east in this image for an east-west distance of ~ 900 km.

2.2. Multipoint Ionosonde Observations

[10] To see ionospheric disturbances associated with the 630-nm airglow enhancements, we checked 15-min resolution ionograms obtained by the three ionosondes shown in Figure 1. Figures 5e and 5f show virtual heights at 2 MHz and f_oF_2 frequencies, respectively, obtained at Wakkanai, Kokubunji, and Okinawa during the 630-nm airglow enhancements of 15 September 1999. The virtual height at 2 MHz and the f_oF_2 frequency correspond to the representative height of the nighttime bottomside F layer and the square root of the peak electron density of the F layer, respectively. For comparison, these parameters for a magnetically quiet day (6 September 1999, sum $Kp = 11+$) and

from the International Reference Ionosphere (IRI) 95 are also shown in Figures 5a–5d.

[11] Clear negative excursions of virtual height can be seen in Figure 5f at all three stations at 1300–1500 UT (2200–2400 LT) on 15 September. The maximum decrease in height was 160 km at Kokubunji from 1245 to 1500 UT. These negative excursions propagate equatorward; i.e., they were observed first at Wakkanai and last at Okinawa. By taking a negative peak at 1415 UT at Wakkanai and 1500 UT at Kokubunji, we estimate the equatorward velocity of propagation to be ~ 400 m/s. It is quite likely that this F layer descent caused the observed airglow enhancement by pushing the high-density plasma at the F layer peak (~ 400 km) into the airglow emission layer at ~ 250 km.

[12] It is noteworthy that the time lag from Wakkanai to Okinawa was also observed at the rising phase of the virtual height at 0900–1200 UT. This rise of the layer in the evening was also observed during the quiet day of 6 September and in the IRI-95 model and may correspond to the decrease in electron density after sunset. The time lag from Wakkanai to Okinawa is also seen in the IRI-95 model, because of the longitudinal and latitudinal difference between the stations (Wakkanai is eastward of Okinawa and at a higher latitude). However, the time lag of the rise of the layer tends to be opposite in the 6 September data.

[13] The f_oF_2 frequencies clearly increase in Figure 5e with decreasing virtual height for 1300–1500 UT on September 15. Such enhancement is not seen in the data of 6 September and IRI-95. The enhancement was 2–3 MHz (30–40% from background values), which corresponds to an enhancement of F layer peak electron density N_{max} of 70–100%, since f_oF_2 is proportional to the square root of N_{max} . For all three stations the peak of f_oF_2 almost coincides with the minimum of the virtual height.

2.3. Total Electron Content (TEC)

[14] For the ionospheric electron density, GPS-TEC measurements carried out by the Geographical Survey Institute, Japan, give useful results, since the Institute has more than 1000 GPS receivers over Japan [Saito *et al.*, 1998]. Figure 6 shows maps of the TEC variations with a time resolution of 10 min, obtained using three GPS satellites (PRN03, 22, and 31) during the 630-nm airglow enhancement of 15 September 1999. A running average of TEC over 1 hour was subtracted from the raw TEC values and plotted in Figure 6, in order to avoid the effect of changing line-of-sight elevation angles due to the satellite motion [Saito *et al.*, 1998]. The mapped TEC values are located at an altitude of 250 km.

[15] An east-west band structure of TEC enhancement can be seen in Figure 6 for 2300–0000 LT (1400–1500 UT). The structure moved equatorward continuously. The estimated equatorward velocity was ~ 430 m/s. The maximum amplitude of the TEC enhancement was $\sim 1.0 \times 10^{16} \text{ m}^{-2}$. Because the background TEC values at 1400–1500 UT for 32°N – 44°N were 22 – $15 \times 10^{16} \text{ m}^{-2}$ (estimated by the method of Otsuka *et al.* [2002]), the TEC enhancement corresponds to ~ 5 – 7% of the background TEC values. The meridional width of the band structure was more than 1000 km. This horizontal size

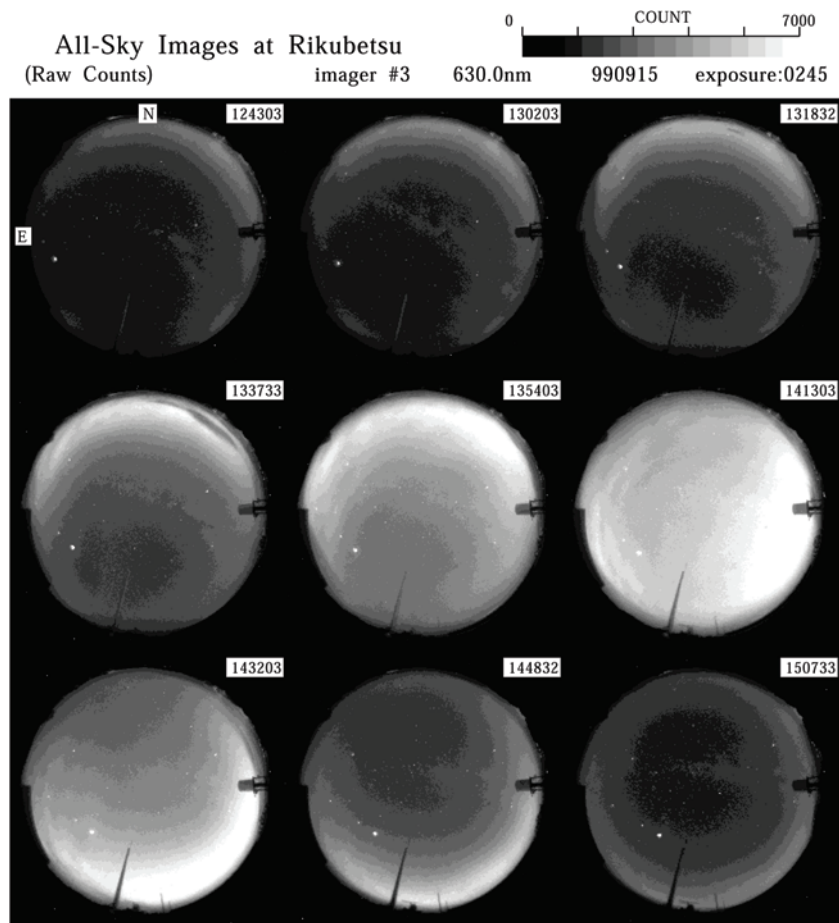


Figure 4. All-sky images at a wavelength of 630 nm obtained at Rikubetsu during the passage of the large-scale traveling ionospheric disturbance (LSTID) of 15 September 1999. North is upward, and east is to the left. The LSTID passed over Rikubetsu from north to south at 1300–1500 UT (2200–2400 LT). See color version of this figure at back of this issue.

may be underestimated by the procedure of the 1-hour running-average subtraction.

2.4. Magnetic Field Variations

[16] To see geomagnetic activities during the observed LSTID event, we plotted the H component magnetic field variations of 15 September 1999, in Figure 7. The data (210° magnetic meridian chain data, see *Yumoto and the 210° MM Magnetic Observation Group* [1996] for details) were obtained mostly in the Japanese meridian of 2200–2400 magnetic local times (MLTs) from Siberia (auroral zone: KTN, TIX, and CHD), southern Siberia (ZYK and PTK), Japan (MSR, RIK, and KAG), to Indonesia (BIK). Low-latitude data at the early morning sector at Hawaii (EWA, 0310 MLT) are also shown.

[17] If the LSTID observed by optical and radio techniques in Figures 3–6 was generated in the auroral zone at $\sim 65^\circ$ N MLAT, it would be initiated around 1200 UT, because the event was observed at ~ 1400 UT at 34.7° N MLAT (Rikubetsu) and moved southward with a velocity of ~ 400 – 450 m/s (~ 1500 km/h). Looking at the high-latitude magnetogram in Figure 7, a small substorm can be identified for 1140–1230 UT with a negative H bay of ~ 200 nT at Chokurdakh (CHD). Positive H excursions, which are usually seen in the low-latitude magnetogram associated

with substorms, can be identified at the low-latitude stations at this time. Around 1000 UT, an intense substorm was observed with clear negative H variations at Kotel'nyy (KTN) and CHD and positive H excursions of ~ 20 nT at most of the low-latitude stations.

2.5. Auroral Activities

[18] To see the substorm feature at 1140–1230 UT more clearly, we show ultraviolet auroral images obtained by the Polar UVI instrument [*Torr et al.*, 1995] in Figure 8. The images are on the MLT-MLAT map with a time resolution of 11 min. The local times of the Japanese meridian are indicated by the arrows. The intense polar cap emission for 1500–2100 MLT is scattered sunlight. The onset of an auroral substorm can be identified between 1140:36 and 1151:39 UT. The whole nightside oval was intensified around 1202 UT. A poleward moving surge structure was seen at 1213–1235 UT at around 2000–2300 MLT between 60° and 75° MLAT.

3. Discussion

3.1. Comparison With the Midlatitude Ionospheric Model

[19] The airglow enhancement was probably caused by the observed sudden decrease of F layer height associated

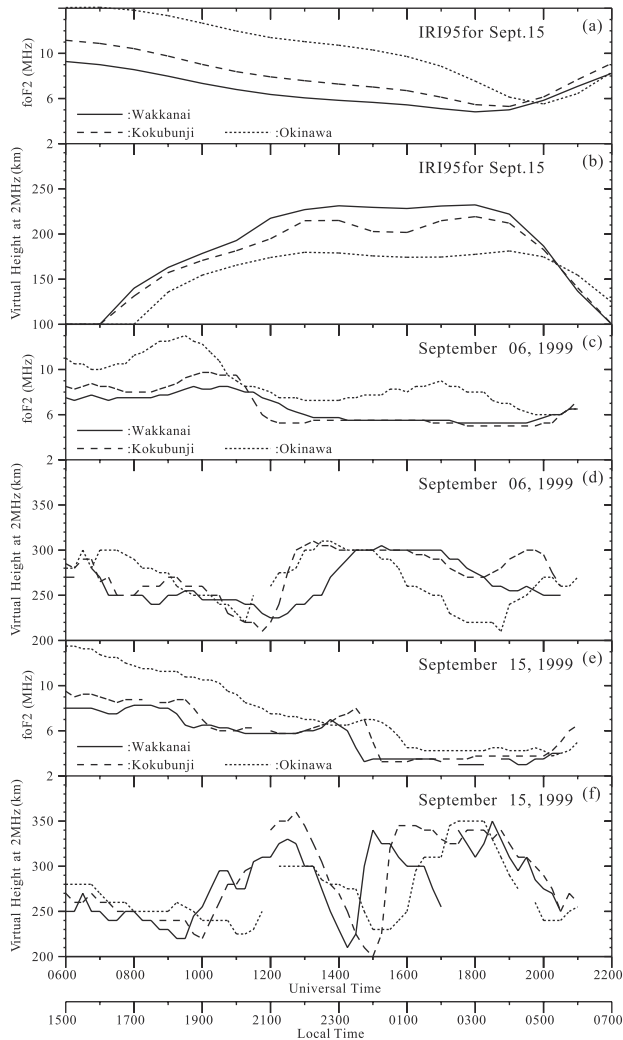


Figure 5. Variations in the F region virtual height at 2 MHz and f_oF_2 values obtained at three ionosonde stations in Japan during the large-scale traveling ionospheric disturbance (LSTID) of (e and f) 15 September 1999 during the magnetically quiet interval of (c and d) 6 September 1999 and calculated from the IRI-95 model for parameters of (a and b) 15 September 1999. Note that the ordinate scale in Figure 5b is different from that of Figures 5d and 5f. The station locations are shown in Figure 1. The nighttime virtual heights after ~ 1800 LT are those at 2 MHz, while the daytime virtual heights before ~ 1800 LT are the real virtual heights. The passage of the LSTID from north to south was identified as decreases of the virtual heights in Figure 5f and increases of the f_oF_2 values in Figure 5e at 1300–1500 UT (2200–2400 LT) on 15 September.

with the LSTID passage, supplying high-density plasma around the F layer peak (~ 400 km) to the airglow emission layer (~ 250 km). The reduced height of the F layer at midlatitudes has two possible causes: the westward electric field and the poleward neutral wind. If the electric field is the cause, it would be imposed on the ionosphere simultaneously on a global scale, because the electric field associated with magnetic activity is penetrated by magneto-

spheric processes. However, because there was a time lag in the decrease of the layer height from Wakkanai to Okinawa (Figure 5), the decrease was probably caused by the poleward neutral wind propagating equatorward as a gravity wave in the thermosphere. As shown in the schematic picture of Figure 9, the horizontal poleward neutral wind can push the plasma downward along the magnetic field line at midlatitudes, where the field line has a finite angle to the horizontal plane.

[20] In order to check the relations between the observed changes in the virtual height, f_oF_2 , airglow emission, and GPS-TEC during the LSTID passage, we performed a model calculation using the Sheffield University Plasma-sphere-Ionosphere Model (SUPIM) [Bailey and Balan, 1996]. By putting an artificial poleward wind of 200 m/s with a temperature increase of 200 K for 2200–2345 LT at the Northern Hemisphere of 24° – 56° MLAT into the model, we checked how the ionospheric parameters are changed. The 200 K temperature change is adopted because most of the LSTID models predict the temperature enhancement, although the results without temperature change are not much difference to those with the change in our model. For background neutral atmosphere and its horizontal wind we used mass spectrometer incoherent scatter 1986 (MSIS-86) [Hedin, 1987] and HWM90 [Hedin et al., 1991], respectively, with $F_{10.7} = 151$ and $A_p = 27$ for 15 September 1999, at 34° MLAT (Rikubetsu). The column airglow emission at O I (630 nm) was calculated using chemical reaction parameters given by Sobral et al. [1993] (same method to that of Ogawa et al. [2002]). The GPS-TEC value was calculated by integrating electron density from the bottomside of the ionosphere to the altitude of the GPS satellites [Balan et al., 2002].

[21] Figure 10 shows the results of the model calculation. The artificial poleward wind (200 m/s) is imposed at 2200–2345 LT on the slowly varying meridional wind given by HWM90. Owing to this poleward wind, h_{max} decreases from 350 to 240 km (-110 km), N_{max} increases from $3.0 \times 10^5 \text{ cm}^{-3}$ to $4.5 \times 10^5 \text{ cm}^{-3}$. Table 1 summarizes the observed and calculated changes in virtual height, N_{max} , airglow intensity, and GPS-TEC values before and during the LSTID passage. The changes in these parameters are fairly well reproduced by the model with the 200 m/s poleward wind, although the model tends to estimate higher than observed values for the column-integrated airglow and TEC on this night. The difference in TEC may be because we underestimate the amplitude in the observed TEC due to the subtraction of a running average of 1 hour from the raw TEC data.

[22] For reference, the changes with 100 m/s poleward wind and 200 m/s equatorward wind are also listed in Table 1. The equatorward wind enhancement causes ionospheric F layer rise along the local magnetic field line and subsequent airglow decrease, as expected. Since the layer rise results in decrease of recombination at lower altitudes, it causes a slight enhancement of N_{max} and GPS-TEC.

[23] The reasons that N_{max} and TEC are increased by the 200 m/s poleward neutral wind are explained as follows. Schematic picture of the physical mechanisms is shown in Figure 9. When the poleward wind is suddenly enhanced in

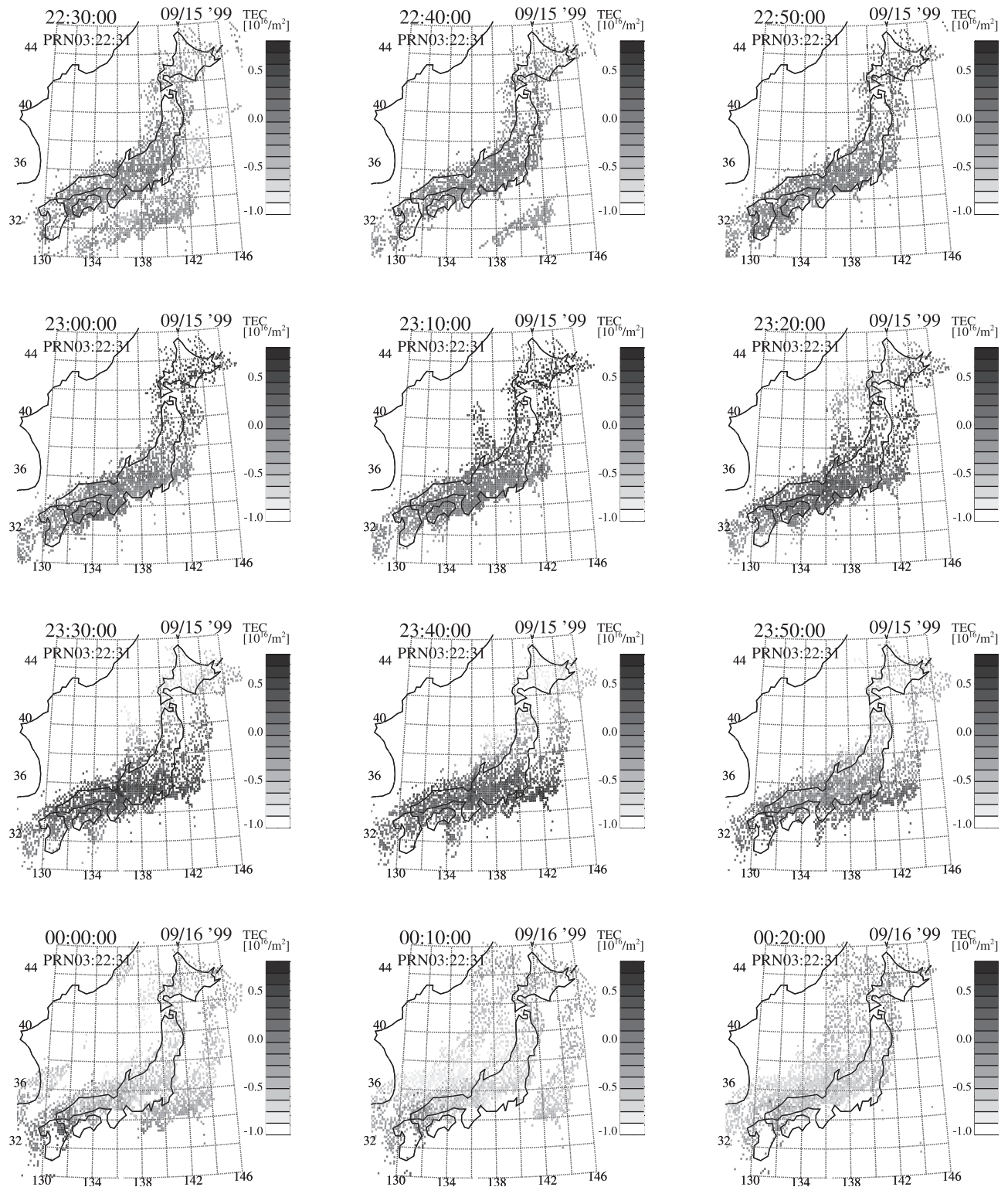


Figure 6. Two-dimensional maps of the total electron content (TEC) variations obtained by more than 1000 GPS receivers in Japan during the passage of the large-scale traveling ionospheric disturbance (LSTID) of 15 September 1999. A running average of TEC over 2 hours was subtracted from the raw TEC values, in order to avoid the effect of changing line-of-sight elevation angles due to the satellite motion. Three GPS satellites (PRN 03, 22, and 31) were used to obtain the TEC values, which are mapped at an altitude of 250 km. See color version of this figure at back of this issue.

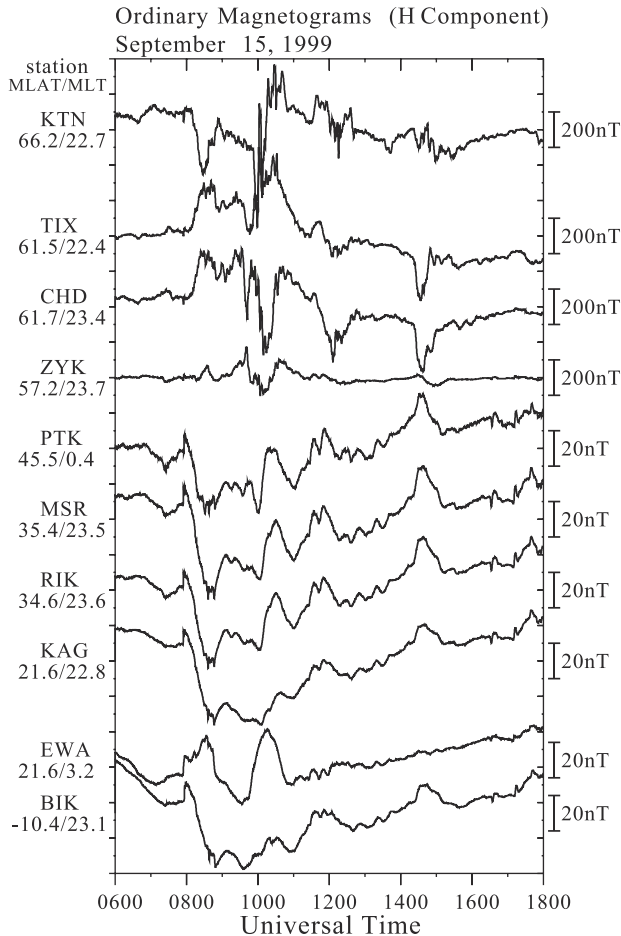


Figure 7. H component magnetic field variations observed at high- and low-latitude stations along the Japanese meridian for 0600–1800 UT on 15 September 1999. Station names, magnetic latitudes (MLAT), and magnetic local times (MLT) at 1400 UT are shown at the left side of the panels, where KTN, TIX, CHD, ZYK, PTK, MSR, RIK, KAG, EWA, and BIK are Kotel’nyy, Tixie, Chokurdakh, Zyryanka, St. Paratunka, Moshiri, Rikubetsu, Kagoshima, Ewa Beach, and Biak, respectively.

the midlatitude ionosphere, the whole ionospheric plasma is pushed downward along the magnetic field line. Then, the loss of the plasma at the topside ionosphere is compensated by downward plasma flow from the plasmasphere, which in turn is balanced by plasma flow from the other hemisphere. Thus the total plasma density (TEC) is temporarily increased by this plasma supply from higher altitudes. Then, the TEC decreases gradually owing to the recombination of plasma at lower altitudes. The reason why TEC does not increase with the 100 m/s poleward wind in Table 1 is because this recombination effect overcomes the effect of plasma supply for weaker wind.

[24] The poleward wind enhancement can also cause a temporal enhancement of N_{\max} to keep the vertical pressure balance. Namely, the downward force by the ion neutral collision should be balanced by an enhanced upward pressure gradient, which results in steepening of the topside ionosphere and enhancement of N_{\max} . This concept can be

expressed by the equation of force balance along the magnetic field line as follows:

$$-m_i g \sin I - \frac{2k_B T}{n} \frac{\partial n}{\partial s} - m_i \nu_{in} (v_{i,\parallel} - v_n \cos I) = 0, \quad (1)$$

where m_i is ion mass, g is the acceleration of gravity, I is the inclination of the magnetic field line, k_B is Boltzmann’s constant, T is ion temperature, n is ion density, s is distance along the field line, ν_{in} is the collision frequency between ions and neutrals, $v_{i,\parallel}$ is the ion velocity along the field line, and v_n is the horizontal neutral wind velocity. The first, second, and third terms express the gravitational force, pressure gradient force, and collisional force due to the velocity difference between ions and neutrals, respectively. The sudden enhancement of v_n should be balanced by enhancement of the density gradient $\partial n/\partial s$ if the temperature gradient is constant. This steepening of density gradient will cause a temporal enhancement of N_{\max} . In other words, due to the neutral wind enhancement, the ionospheric plasma is compressed into a narrower layer in the lower altitudes and the local ion density around the peak increases, as shown in Figure 9. Then, N_{\max} decreases gradually by recombination with the rich neutral atmosphere in the lower altitudes, as shown in Figure 10 after 2230 LT. For the case of weaker poleward wind (100 m/s) this recombination effect again overcomes the effect of the compression and results in the N_{\max} decrease, as listed in Table 1.

[25] The above discussion does not include the effect of plasma accumulation by vertical structure of gravity waves discussed by *Hooke* [1968]. Simple estimation of vertical wavelength λ_z of gravity wave for the present event will be $\lambda_z = 360$ km (which is horizontal phase velocity 400 m/s \times Brunt-Väisälä period 15 min), which is comparable to the thickness of the F layer and preferable to the plasma accumulation effect. However, the actual λ_z may be much larger owing to the molecular dissipative effect, as shown in Figure 7 by *Richmond* [1978].

[26] From these considerations of physical mechanisms and the result of the comparison in Table 1, we conclude that the observed features of the LSTID passage, i.e., airglow intensification, virtual height decrease, f_oF_2 increase, and GPS-TEC increase, are caused by an enhancement of the poleward neutral wind (250–300 m/s). We suggest that this enhancement of the poleward wind (that propagates equatorward) is caused by an equatorward propagating gravity wave in the thermosphere. In section 3.2 we discuss how this gravity wave is generated in the high-latitude auroral zone.

3.2. Source in the Auroral Zone

[27] The LSTID event was observed around 1400 UT at 34.7°N MLAT (Rikubetsu) with a southward velocity of ~ 400 –450 m/s (~ 1500 km/h). Backtracing this motion to the auroral zone, the source of the LSTID must be around 1200 UT. As shown in Figure 7 and Figure 8, there was a small substorm at this time. In order to see the energy input in the auroral zone, we show the auroral Joule heating rate and cross polar cap potential calculated by the AMIE technique [*Richmond and Kamide*, 1988] in Figure 11. The AMIE procedure calculates these parameters from ground magnetometer data using the inversion technique

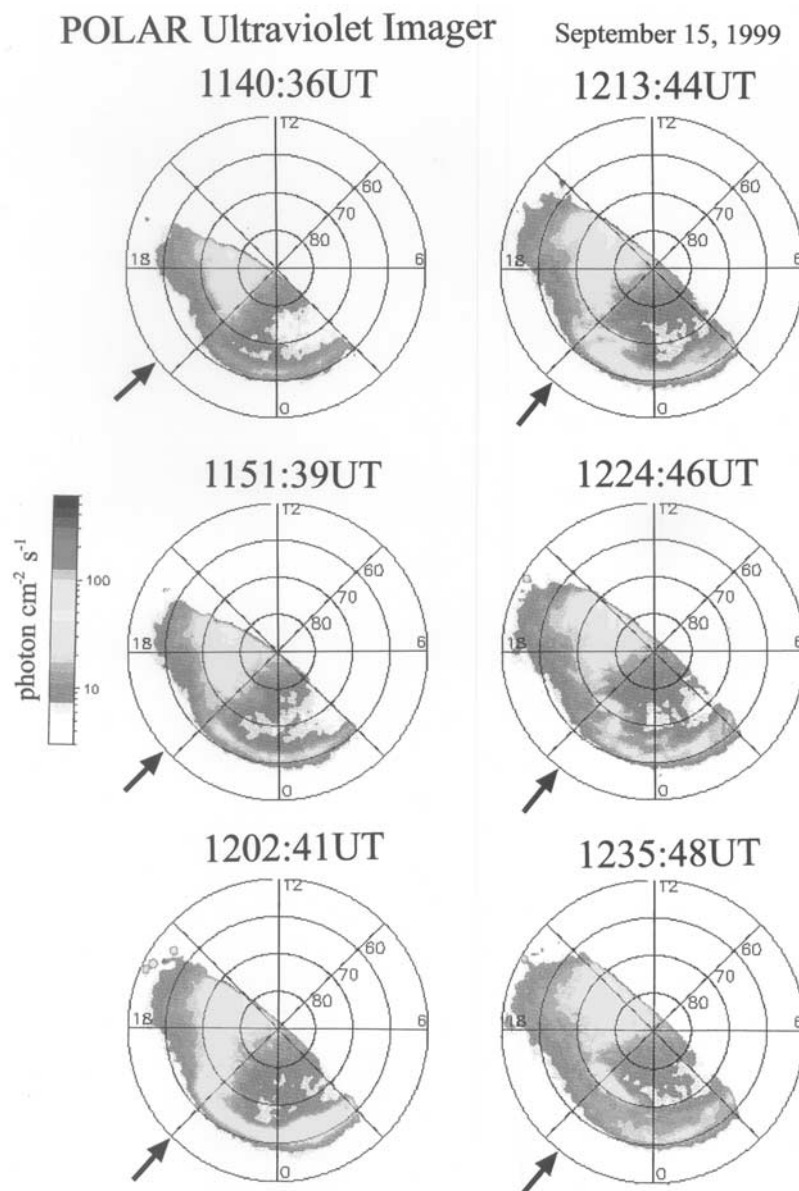


Figure 8. Auroral images on the MLT-MLAT maps obtained by the Polar UVI imager at 1140–1235 UT on 15 September 1999. The intense polar cap emission for 1500–2100 MLT is scattered sunlight. An auroral substorm took place between 1140:36 and 1151:39 UT. The nightside oval is intensified around 1202 UT. The arrows indicate local times of the Japanese meridian. See color version of this figure at back of this issue.

by considering the ionospheric conductivity. The high-latitude magnetometer data shown in Figure 7 are also used in this empirical model.

[28] Figure 11 shows that the Joule heating rate during this small substorm at 1140–1230 UT was less than 200 GW, which is far lower than the Joule heating rate during the two major substorms at 0800–0900 UT and 1000–1100 UT. It is not likely that this small substorm caused the observed prominent LSTID at midlatitudes. Moreover, a simple auroral energy input causes equatorward wind instead of poleward wind owing to expansion of the heated atmosphere.

[29] Some LSTID simulations with auroral energy input predict poleward wind enhancement after the passage of

initial equatorward wind [e.g., *Richmond, 1978; Millward et al., 1993*]. The intense poleward wind observed in the present case may correspond to this case, after the intense auroral energy inputs at 0800–0900 UT and 1000–1100 UT in Figure 11 cease. The F layer rise at 1000–1200 UT in Figure 5f might be the signature of initial equatorward wind by the LSTID. However, a similar rise from Wakkanai to Okinawa was seen in the IRI95 model in Figure 5b, because of the difference of the sunset times at these stations. It is difficult to distinguish these two effects for the layer rise. It is interesting that the signatures of the F layer descent at 1300–1500 UT are much more drastic than those of the rise at 1000–1200 UT. The f_oF_2 enhancement was observed only at 1300–1500 UT, in association with the layer

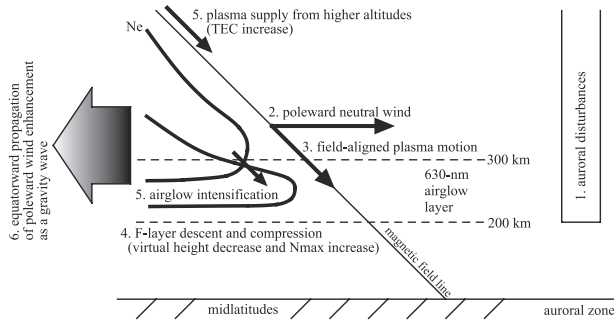


Figure 9. Schematic diagram of the physical processes suggested in this paper on the basis of the LSTID observation and model calculation. The number preceding each comment indicates the order of occurrence. The poleward neutral wind is generated as a gravity wave probably by some disturbances in the auroral zone. The poleward wind pushes plasma downward along the local magnetic field line, resulting in the F layer descent and compression. The F layer descent causes oxygen airglow intensification at 630 nm by supplying plasma into lower altitudes where the atomic oxygen density is high. The peak electron density N_{\max} temporally increases owing to the compression. (It then decreases owing to the recombination at lower altitudes). The loss of the plasma at the topside ionosphere due to the layer descent is compensated by the plasma supply from higher altitudes and from the conjugate hemisphere, resulting in the temporal enhancement of the total electron content. The whole process propagates equatorward associated with the equatorward motion of the atmospheric gravity wave that causes the poleward wind enhancement.

descent. Comparison with global LSTID generation models will be necessary for further discussion.

[30] The other possibility is the Lorentz force. As discussed by Hunsucker [1982], the Lorentz force ($\mathbf{J} \times \mathbf{B}$), where \mathbf{J} is the current density and \mathbf{B} is the magnetic field intensity, can be transferred to the neutral gas via

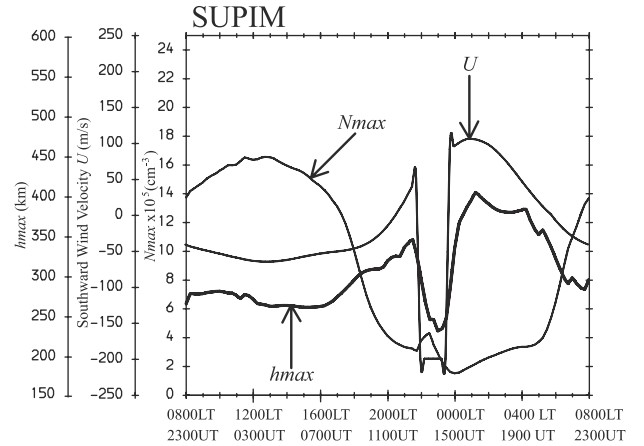


Figure 10. Variations in the peak electron density (N_{\max}) and peak height (h_{\max}) of the ionospheric F layer, calculated by the Sheffield University Plasmasphere-Ionosphere Model (SUPIM) for a sudden decrease (250–300 m/s) in southward neutral wind velocity (U) at 2200–2345 UT on 15 September 1999. The U values for other time intervals are given by the HWM90 model.

collisions and cause LSTIDs. In the Polar UVI auroral images, there was a clear poleward motion of auroral surge structure at 1213–1235 UT (Figure 8). This poleward motion may be an indication of the poleward Lorentz force that results in the enhancement of the poleward neutral wind. However, the negative H bay in the auroral zone magnetogram (CHD) in Figure 7 was not so intense at 1140–1230 UT, suggesting that the amount of \mathbf{J} for the $\mathbf{J} \times \mathbf{B}$ force was not so large.

4. Conclusions

[31] We have used a comprehensive dataset to investigate the dynamics, propagation, and source mechanisms of a prominent LSTID event observed in Japan during the magnetic storm of 15 September 1999. The observed

Table 1. Comparison Between Observed and Calculated Ionospheric Parameters Before and During the LSTID Event

	Virtual Height	N_{\max}	Airglow Intensity	GPS-TEC
		<i>Observed</i>		
Difference	–120 km ^a	$\sim 1.6 \times 10^5 \text{ cm}^{-3\text{b}}$	$\sim 300 \text{ R}$	$\sim 1.0 \times 10^{16} \text{ m}^{-2}$
Before	330 km (2130 LT) ^a	$\sim 4.5 \times 10^5 \text{ cm}^{-3}$ (2145 LT) ^b	$\sim 50 \text{ R}$ (2220 LT)	–
During	210 km (2315 LT) ^a	$\sim 6.1 \times 10^5 \text{ cm}^{-3}$ (2245 LT) ^b	$\sim 350 \text{ R}$ (2310 LT)	–
		<i>Calculated^c (200 m/s Poleward Wind, Figure 10)</i>		
Difference	–110 km	$1.5 \times 10^5 \text{ cm}^{-3}$	330 R	$3.6 \times 10^{16} \text{ m}^{-2}$
Before	350 km (2130 LT)	$3.0 \times 10^5 \text{ cm}^{-3}$ (2145 LT)	140 R (2145 LT)	$16.2 \times 10^{16} \text{ m}^{-2}$ (2145 LT)
During	240 km (2300 LT)	$4.5 \times 10^5 \text{ cm}^{-3}$ (2230 LT)	470 R (2215 LT)	$19.8 \times 10^{16} \text{ m}^{-2}$ (2215 LT)
		<i>Calculated^c (100 m/s Poleward Wind)</i>		
Difference	–90 km	$-0.7 \times 10^5 \text{ cm}^{-3}$	49 R	$-2.5 \times 10^{16} \text{ m}^{-2}$
		<i>Calculated^c (200 m/s Equatorward Wind)</i>		
Difference	+100 km	$0.1 \times 10^5 \text{ cm}^{-3}$	–70 R	$1.1 \times 10^{16} \text{ m}^{-2}$

^a At 2 MHz at Wakkanai.

^b At Wakkanai, $N_{\max} \text{ cm}^{-3} = 1.24 \times 10^4 [f_oF_2(\text{MHz})]^2$.

^c Values at Rikubetsu.

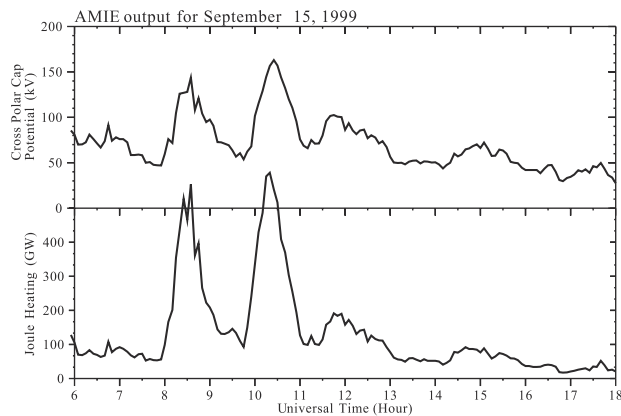


Figure 11. Global Joule heating rate in the auroral zone and cross polar cap potential calculated by the assimilative mapping of ionospheric electrodynamics (AMIE) technique for 0600–1800 UT on 15 September 1999.

features of the LSTID and results from the model calculations are summarized as follows.

1. A prominent airglow enhancement from 50 to 350 R propagating equatorward was observed by a meridian-scanning photometer and an all-sky airglow imager at 2300–2400 LT (1400–1500 UT) at Rikubetsu (34.7°MLAT, MLAT), Japan. The equatorward velocity estimated by the photometer data was ~ 450 m/s.

2. The F layer virtual height at 2 MHz decreases from 360 to 200 km at three ionosonde stations in Japan. The f_oF_2 value increases from ~ 6 to ~ 8 MHz ($N_{\max} \sim 4.5 \rightarrow 7.9 \times 10^5 \text{ cm}^{-3}$, values at Kokubunji). These variations propagate equatorward with a velocity of ~ 400 m/s.

3. The GPS-TEC maps over Japan show an east-west band structure of TEC enhancement with a meridional scale size of more than 1000 km propagating equatorward with a velocity of ~ 430 m/s. The TEC enhancement was $\sim 1.0 \times 10^{16} \text{ m}^{-2}$, which is ~ 5 –7% of the total TEC.

4. Ground magnetic field data and Polar UVI auroral images show that a small substorm took place at 1140–1230 UT, which is consistent with the onset time of the LSTID estimated by backtracing the LSTID propagation to the auroral zone.

5. From a comparison with the results of a SUPIM calculation, we conclude that these observed features of the LSTID passage, i.e., airglow intensification, decrease in virtual height, increase in f_oF_2 , and increase in GPS-TEC, are caused by an enhancement of poleward neutral wind (250–300 m/s). We suggest that this enhancement of the poleward wind (that propagates equatorward) is caused by an equatorward propagating gravity wave in the thermosphere.

6. The auroral Joule heating rate calculated by the AMIE procedure suggests that the substorm at 1140–1230 UT does not cause significant Joule heating to produce the observed prominent LSTID. The atmospheric gravity wave that can be generated associated with the cessation of the intense auroral energy input at 0800–1100 UT, is likely to be a cause of the poleward wind enhancement.

[32] **Acknowledgments.** We thank M. K. Ejiri, Y. Katoh, M. Satoh, and T. Katoh of the Solar-Terrestrial Environment Laboratory, Nagoya

University, for their kind support in the development of the all-sky imager and the meridian-scanning photometer. The magnetic field data used in this paper were supplied by the 210 magnetic meridian magnetic observation project. The multipoint GPS data were supplied by the Geographical Survey Institute, Japan. The POLAR UVI images were supplied through the NASA MSFC home page. K. S. is grateful to T. Maruyama for his helpful comments. This work was supported by Grant-in-Aid for Scientific Research of the Ministry of Education, Culture, Sports, Science and Technology of Japan (11440145).

[33] Janet G. Luhmann thanks George Millward and another referee for their assistance in evaluating this paper.

References

- Afraimovich, E. L., E. A. Kosogorov, L. A. Leonovich, K. S. Palamartchouk, N. P. Perevalova, and O. M. Pirog, Observation of large-scale traveling ionospheric disturbances of auroral origin by global GPS networks, *Earth Planets Space*, **52**, 669–674, 2000.
- Bailey, G. J., N. Balan, A low-latitude ionosphere-plasmasphere model, in *STEP Handbook*, edited by R. W. Schunk, p. 173, Utah State Univ., Logan, 1996.
- Balan, N., Y. Otsuka, T. Tsugawa, S. Miyazaki, T. Ogawa, and K. Shiokawa, Plasmaspheric electron content in the GPS ray paths over Japan, *Earth Planets Space*, **54**, 71–79, 2002.
- Balthazor, R. L., and R. J. Moffett, Morphology of large-scale traveling atmospheric disturbances in the polar thermosphere, *J. Geophys. Res.*, **104**, 15–24, 1999.
- Buonsanto, M. J., M. Codrescu, B. A. Emery, C. G. Fesen, T. J. Fuller-Rowell, D. J. Melendez-Alvira, and D. P. Sipler, Comparison of models and measurements at Millstone Hill during the January 24–26, 1993, minor storm interval, *J. Geophys. Res.*, **102**, 7267–7277, 1997.
- Emery, B. A., et al., Assimilative mapping of ionospheric electrodynamics in the thermosphere-ionosphere general circulation model comparisons with global ionospheric and thermospheric observations during the GEM/SUNDIAL period of March 28–29, 1992, *J. Geophys. Res.*, **101**, 26,681–26,696, 1996.
- Emery, B. A., C. Lathuillere, P. G. Richards, R. G. Roble, M. J. Buonsanto, D. J. Knipp, P. Wilkinson, D. P. Sipler, and R. Niciejewski, Time dependent thermospheric neutral response to the 2–11 November 1993 storm period, *J. Atmos. Solar-Terr. Phys.*, **61**, 329–350, 1999.
- Francis, S. H., Global propagation of atmospheric gravity waves: A review, *J. Atmos. Terr. Phys.*, **37**, 1011–1054, 1975.
- Fujiwara, H., S. Maeda, H. Fukunishi, T. J. Fuller-Rowell, and D. S. Evans, Global variations of thermospheric winds and temperatures caused by substorm energy injection, *J. Geophys. Res.*, **101**, 225–239, 1996.
- Fuller-Rowell, T. J., M. V. Codrescu, R. J. Moffett, and S. Quegan, Response of the thermosphere and ionosphere to geomagnetic storms, *J. Geophys. Res.*, **99**, 3893–3914, 1994.
- Hajkowicz, L. A., A global study of large scale travelling ionospheric disturbances (TIDs) following a step-like onset of auroral substorms in both hemispheres, *Planet. Space Sci.*, **38**, 913–923, 1990.
- Hajkowicz, L. A., and R. D. Hunsucker, A simultaneous observation of large-scale periodic TIDs in both hemispheres following an onset of auroral disturbances, *Planet. Space Sci.*, **35**, 785–791, 1987.
- Hedin, A. E., MSIS-86 thermospheric model, *J. Geophys. Res.*, **92**, 4649–4662, 1987.
- Hedin, A. E., et al., Revised global model of thermosphere winds using satellite and ground-based observations, *J. Geophys. Res.*, **96**, 7657–7688, 1991.
- Ho, C. M., A. J. Mannucci, U. J. Lindqwister, X. Pi, and B. T. Tsurutani, Global ionosphere perturbations monitored by the worldwide GPS network, *Geophys. Res. Lett.*, **23**, 3219–3222, 1996.
- Ho, C. M., A. J. Mannucci, L. Sparks, X. Pi, U. L. Lindqwister, B. D. Wilson, B. A. Iijima, and M. J. Reyes, Ionospheric total electron content perturbations monitored by the GPS global network during two Northern Hemisphere winter storms, *J. Geophys. Res.*, **103**, 26,409–26,420, 1998.
- Hocke, K., and K. Schlegel, A review of atmospheric gravity waves and traveling ionospheric disturbances: 1982–1995, *Ann. Geophys.*, **14**, 917–940, 1996.
- Hooke, W. H., Ionospheric irregularities produced by internal atmospheric gravity waves, *J. Atmos. Terr. Phys.*, **30**, 795–823, 1968.
- Hunsucker, R. D., Atmospheric gravity waves generated in the high-latitude ionosphere: A review, *Rev. Geophys.*, **20**, 293–315, 1982.
- Kamide, Y., A. D. Richmond, and S. Matsushita, Estimation of ionospheric electric fields, ionospheric currents, and field-aligned currents from ground magnetic records, *J. Geophys. Res.*, **86**, 801–813, 1981.
- Lu, G., A. D. Richmond, R. G. Roble, and B. A. Emery, Coexistence of ionospheric positive and negative storm phases under northern winter conditions: A case study, *J. Geophys. Res.*, **106**, 24,493–24,504, 2001.

- Mendillo, M., J. Baumgardner, D. Nottingham, J. Aarons, B. Reinisch, J. Scali, and M. Kelley, Investigations of thermospheric-ionospheric dynamics with 6300 Å images from the Arecibo Observatory, *J. Geophys. Res.*, *102*, 7331–7343, 1997.
- Millward, G. H., R. J. Moffett, S. Quegan, and T. J. Fuller-Rowell, Effects of an atmospheric gravity wave on the midlatitude ionospheric *F* layer, *J. Geophys. Res.*, *98*, 19,173–19,179, 1993.
- Ogawa, T., N. Balan, Y. Otsuka, K. Shiokawa, C. Ihara, T. Shimomai, and A. Saito, Observations and modeling of 630 nm airglow and total electron content associated with traveling ionospheric disturbances over Shigaraki, Japan, *Earth Planets Space*, *54*, 45–56, 2002.
- Otsuka, Y., T. Ogawa, T. Tsugawa, A. Saito, S. Miyazaki, and S. Fukao, A new technique for mapping of total electron content using GPS network in Japan, *Earth Planets Space*, *54*, 63–70, 2002.
- Pi, X., M. Mendillo, W. J. Hughes, M. J. Buonsanto, D. P. Sipler, J. Kelly, Q. Zhou, G. Lu, and T. J. Hughes, Dynamical effects of geomagnetic storms and substorms in the middle-latitude ionosphere: An observational campaign, *J. Geophys. Res.*, *105*, 7403–7417, 2000.
- Richmond, A. D., Gravity wave generation, propagation, and dissipation in the thermosphere, *J. Geophys. Res.*, *83*, 4131–4145, 1978.
- Richmond, A. D., and Y. Kamide, Mapping electrodynamic features of the high-latitude ionosphere from localized observations: Technique, *J. Geophys. Res.*, *93*, 5741–5759, 1988.
- Saito, A., S. Fukao, and S. Miyazaki, High resolution mapping of TEC perturbations with the GSI GPS network over Japan, *Geophys. Res. Lett.*, *25*, 3079–3082, 1998.
- Shiokawa, K., Y. Katoh, M. Satoh, M. K. Ejiri, T. Ogawa, T. Nakamura, T. Tsuda, and R. H. Wiens, Development of optical mesosphere thermosphere imagers (OMTI), *Earth Planets Space*, *51*, 887–896, 1999.
- Shiokawa, K., Y. Katoh, M. Satoh, M. K. Ejiri, and T. Ogawa, Integrating-sphere calibration of all-sky cameras for nightglow measurements, *Adv. Space Sci.*, *26*(6), 1025–1028, 2000.
- Sobral, J. H. A., H. Takahashi, M. A. Abdu, P. Muralikrishna, Y. Sahai, C. J. Zamlutti, E. R. DE Paura, and P. P. Batista, Determination of the quenching rate of the O(¹D) by O(³P) from rocket-borne optical (630 nm) and electron density data, *J. Geophys. Res.*, *98*, 7791–7798, 1993.
- Tanaka, T., An important role of electric field reversals for the initiation of Gigahertz scintillations at midlatitude during geomagnetic storms, *J. Geomagn. Geoelectr.*, *39*, 659–676, 1987.
- Torr, M. R., et al., A far ultraviolet imager for the international solar terrestrial physics mission, *Space Sci. Rev.*, *71*, 329–383, 1995.
- Yumoto, K., and the 210° MM Magnetic Observation Group, The STEP 210 (deg) magnetic meridian network project, *J. Geomagn. Geoelectr.*, *48*, 1297–1309, 1996.
-
- N. Balan, Radio and Space Physics Group, Department of Physics, University of Wales, Aberystwyth, Ceredigion SY23 3BZ, UK.
- K. Igarashi, Communications Research Laboratory, 4-2-1, Nukui-Kita, Koganei, Tokyo 184-8795, Japan.
- D. J. Knipp, Department of Physics, U.S. Air Force Academy, Suite 2A25, Fairchild Hall, Colorado Springs, CO 80840, USA.
- T. Ogawa, Y. Otsuka, and K. Shiokawa, Solar-Terrestrial Environment Laboratory, Nagoya University, Toyokawa, 442-8507, Japan. (shiokawa@stelab.nagoya-u.ac.jp)
- A. J. Ridley, The University of Michigan, 1411B Space Research Building, Ann Arbor, MI 48109-2143, USA.
- A. Saito, Graduate School of Science, Kyoto University, Kitashirakawa-Oiwakecho, Sakyo-ku, Kyoto 606-8502, Japan.
- K. Yumoto, Faculty of Science, Kyushu University, 6-10-1, Hakozaki, Higashi-ku, Fukuoka 812-8581, Japan.

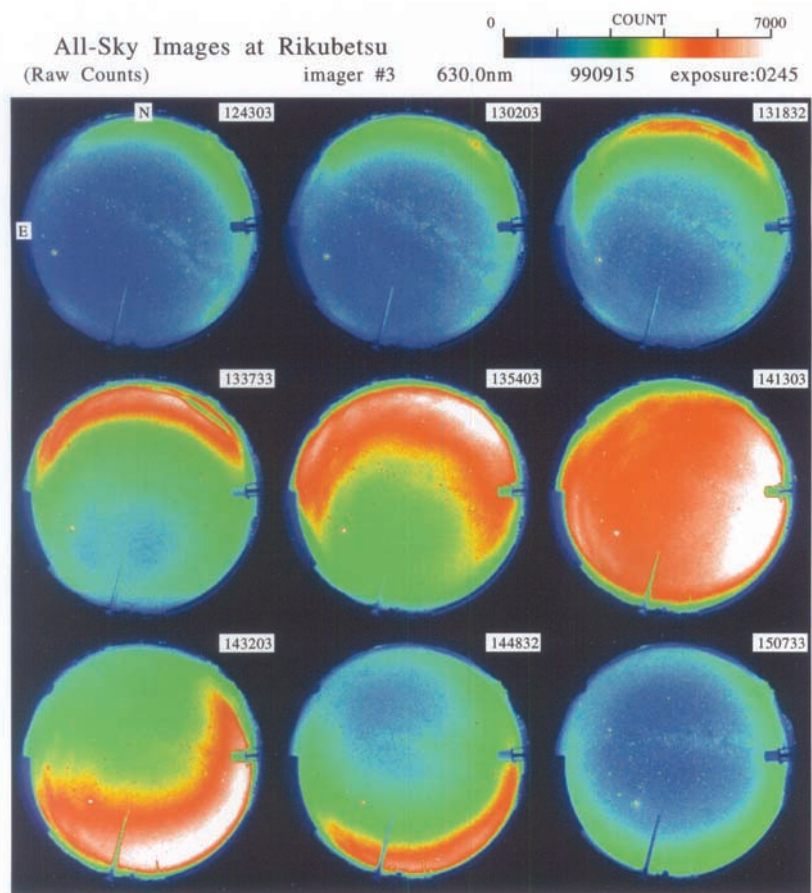


Figure 4. All-sky images at a wavelength of 630 nm obtained at Rikubetsu during the passage of the large-scale traveling ionospheric disturbance (LSTID) of 15 September 1999. North is upward, and east is to the left. The LSTID passed over Rikubetsu from north to south at 1300–1500 UT (2200–2400 LT).

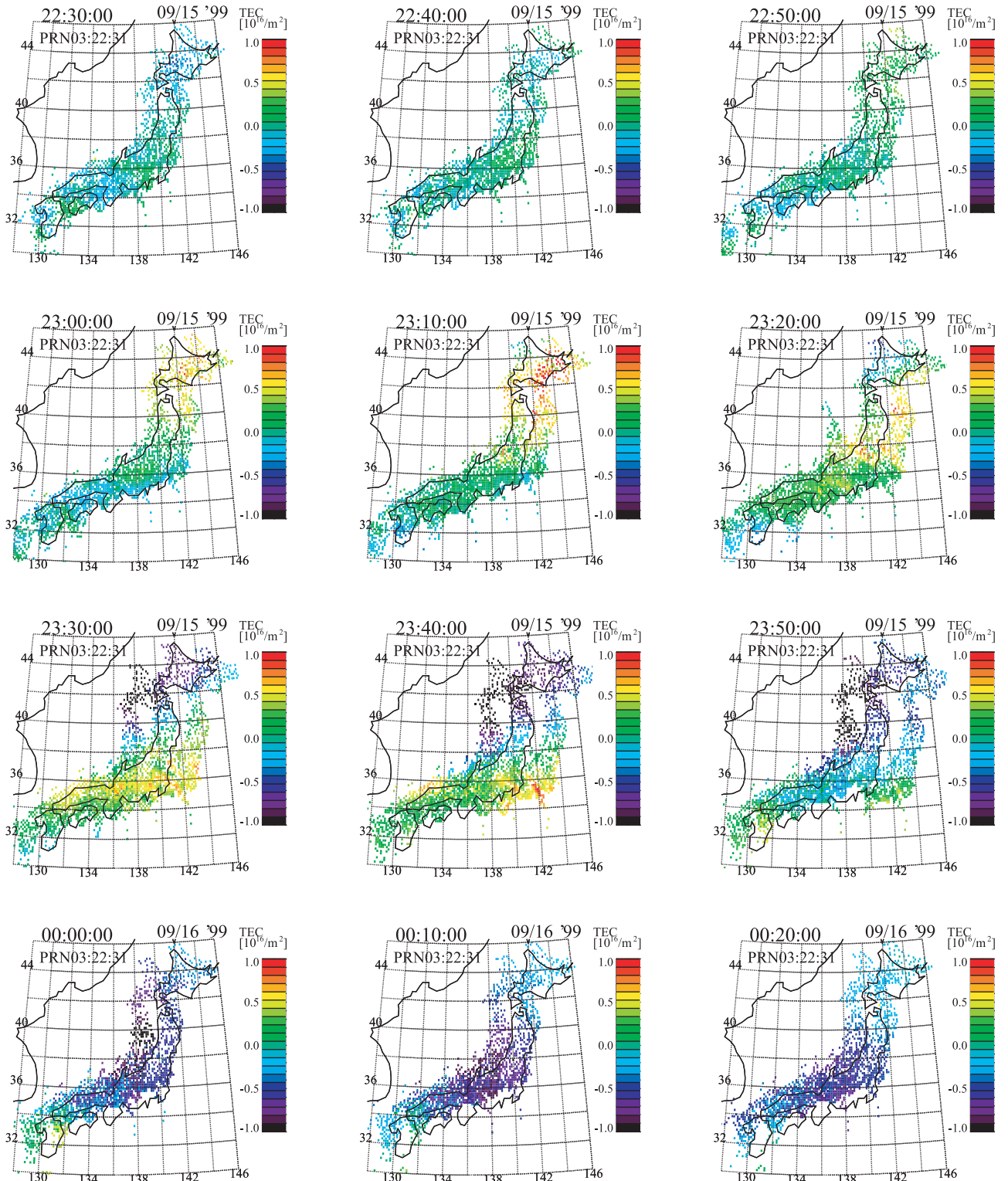


Figure 6. Two-dimensional maps of the total electron content (TEC) variations obtained by more than 1000 GPS receivers in Japan during the passage of the large-scale traveling ionospheric disturbance (LSTID) of 15 September 1999. A running average of TEC over 2 hours was subtracted from the raw TEC values, in order to avoid the effect of changing line-of-sight elevation angles due to the satellite motion. Three GPS satellites (PRN 03, 22, and 31) were used to obtain the TEC values, which are mapped at an altitude of 250 km.

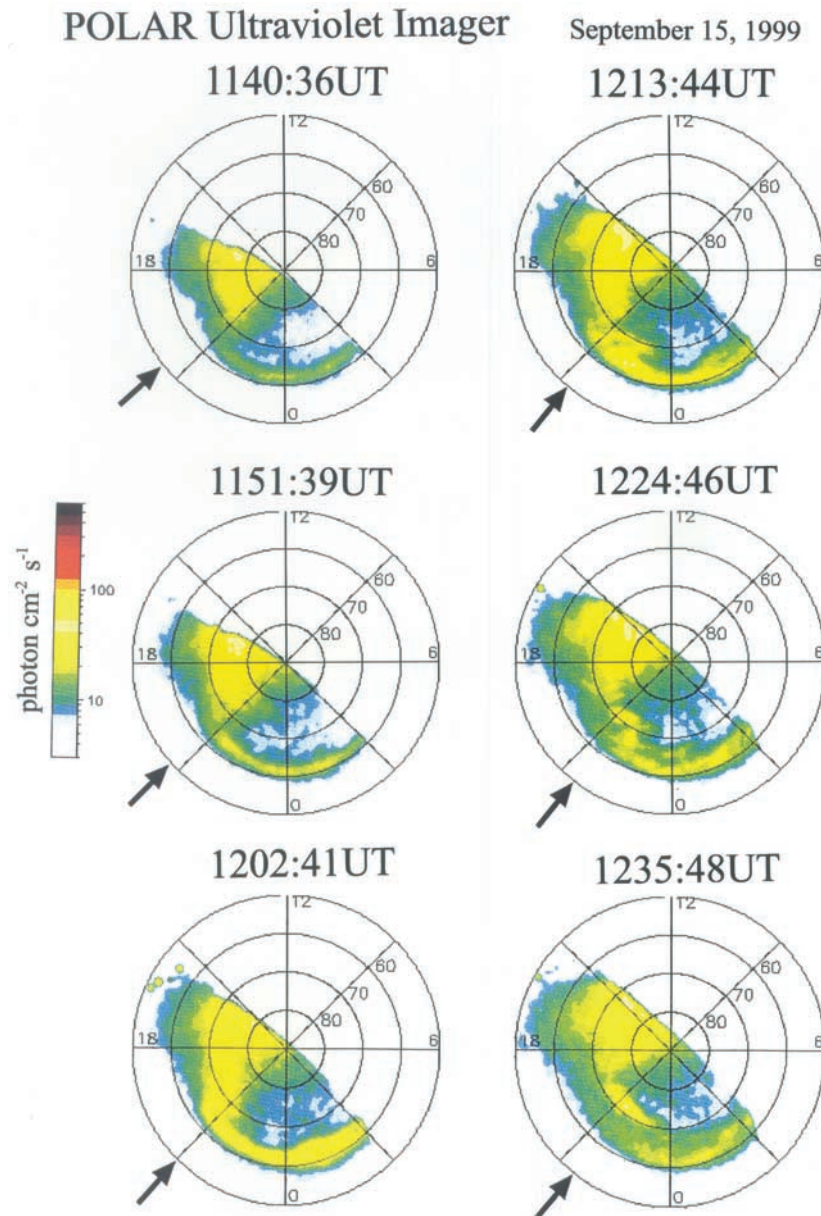


Figure 8. Auroral images on the MLT-MLAT maps obtained by the Polar UVI imager at 1140–1235 UT on 15 September 1999. The intense polar cap emission for 1500–2100 MLT is scattered sunlight. An auroral substorm took place between 1140:36 and 1151:39 UT. The nightside oval is intensified around 1202 UT. The arrows indicate local times of the Japanese meridian.